RAYLEIGH-TAYLOR INSTABILITY: MODELLING AND EFFECT ON COHERENT DEFLAGRATIONS

Keenan, J.J.[1], Makarov, D.V.[1] and Molkov, V.V.[1]
[1] Hydrogen Safety Engineering and Research Centre (HySAFER), University of Ulster, Shore Road, Newtownabbey, Co. Antrim, BT37 0QB,
j.keenan@ulster.ac.uk, dv.makarov@ulster.ac.uk, v.molkov@ulster.ac.uk

ABSTRACT

The modelling of Rayleigh-Taylor instability during premixed combustion scenarios is presented. Experimental data obtained from experiments undertaken by FM Global using their large-scale vented deflagration chamber was used to develop the modelling approach. This development forms an expansion to the multi-phenomena turbulent burning velocity model that is under continuous development at HySAFER. Rayleigh-Taylor instability is introduced as an additional time-dependent, enhancing combustion, mechanism. It is demonstrated that prior to the addition of this mechanism the LES deflagration model under-predicted the pressure transients reported in the experiments, as the intensity of the external deflagration was not fully captured. It is confirmed that the instability plays a significant role throughout the coherent deflagration process due to the flame acceleration that occurs, towards the vent and also during combustion outside the chamber. The addition of the mechanism led to the model more closely replicating the form and the magnitude of the pressure peak associated with the external deflagration.

NOMENCLATURE

$A_{i,t}$	Atwood number (-)	$\lambda_{i,t}$	most unstable wavelength (m)
c	combustion progress variable (-)	μ_{eff}	effective dynamic viscosity (Pa·s)
E	expansion ratio (-)	$\nu_{T,i,t}$	turbulent kinematic viscosity ($m^2/2$)
$g_{i,t}$	acceleration (m/s^2)	Ξ_f	factor representing fractal theory (-)
$h_{0,i,t}$	initial RT amplitude (m)	Ξ_K	self-induced turbulence factor (-)
$h_{i,t}$	RT amplitude at current timestep (m)	Ξ_{lp}	leading point factor (-)
$h_{i,t-\Delta t}$	RT amplitude at previous timestep (m)	Ξ_{RT}	RT instability factor (-)
k_h	constant multiplier (-)	ρ_u	unburned density (kg/m^3)
p	pressure (Pa)	ψ	model constant (-)
R_0	critical radius (m)	$\omega_{i,t}$	growth rate of perturbation (1/s)
S	length of slanted side of cone (m)	***Bars***	
S_1, S_2	surface area 1, surface area 2 (m^2)	$-$	LES filtered quantity
S_c	progress variable source term (kg/m^3-s)	$\sim$	LES mass-weighted filtered quantity
Sc_{eff}	effective Schmidt number (-)	***Subscripts***	
S_T	turbulent burning velocity (m/s)	*c*	source term, progress variable
$S_{T,i,t}$	S_T at current timestep (m/s)	*eff*	effective
$S_{T_x}, S_{T_y}, S_{T_z}$	S_T component in *x, y* and *z* direction	*h*	amplitude
S_u	laminar burning velocity (m/s)	H_2	hydrogen
S_u^w	SGS wrinkled burning velocity (m/s)	*i,j,k*	spatial coordinate indexes
$S_{\Xi_{RT}}$	RT factor source term (1/s)	*T*	turbulent
t	time (s)	*t*	time
T	temperature (K)	*u*	unburned
u'	sub-grid scale velocity (m/s)	*w*	wrinkling
U_x, U_y, U_z	component of flow velocity in x, y and z	$t-\Delta t$	previous timestep
x	spatial coordinate (-)	0	initial conditions
Y_a	mass fraction of air (-)	***Abbreviations***	

Y_{H_2}	mass fraction of hydrogen (-)	CV	control volume
Greek		LES	Large eddy simulation
α	constant coefficient (-)	RNG	renormalization group
Δ_{cv}	ignition CV size (m)	RT	Rayleigh-Taylor
Δt	timestep (s)	SGS	sub-grid scale
Δt_{ign}	time of ignition (s)	UDF	user defined function
ε	thermokinetic index (-)	UDS	user defined scalar

1.0 INTRODUCTION

The goal of this study is to understand the role of Rayleigh-Taylor (RT) instability within the underlying physical phenomena associated with coherent deflagrations (the simultaneous development of internal and external combustion). Following from this, a Large Eddy Simulation (LES) modelling approach, including a mechanism to account for RT instability, has been developed utilising the multi-phenomena turbulent burning velocity model [1], [2]. The importance of the so-called "external explosion" was demonstrated, for the first time, by the numerical analysis of the SOLVEX experiments [3]. During the study [4] of a hydrogen-air deflagration in the congested environment of a mock-up refuelling station [5], RT instability was identified as being the most likely missing mechanism which would, if implemented into the deflagration model [1], contribute to combustion enhancement in flame front areas where there was significant flame front acceleration in the direction from combustion products to the fresh mixture (light into heavy). Following this conclusion, the primary purpose of this paper is to present an extension to the multi-phenomena turbulent burning velocity deflagration model, concentrating on the development of the model to take the increase in the flame front area produced by RT instability into account. This extension to the model was then tested against the experimental results published in [6].

2.0 VALIDATION EXPERIMENTS

The experiments as described by Bauwens et al. [6] were performed using the FM Global 63.7 m^3 large scale test chamber. The overall dimensions of the test chamber were 4.6x4.6x3.0 m with a square vent of 2.7 m^2 or 5.4 m^2 located on one of the vertical walls. In the analysed experiments the hydrogen concentration in air was 18% by volume for both the 2.7 m^2 and 5.4 m^2 vent area experiments. Ignition occurred at either the centre of the back wall of the chamber (0.25 m out from the wall) or at the centre of the chamber, at a height of 1.5 m from the base of the chamber for both ignition locations. The dimensions and overall layout of the experimental setup is shown in Fig. 1.

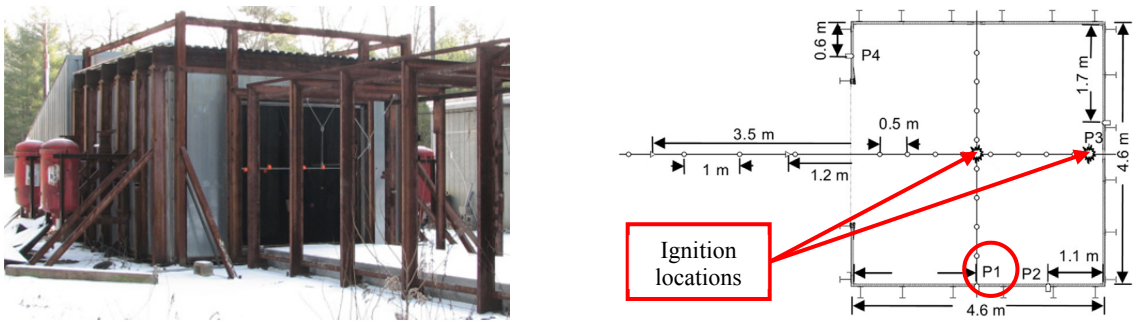

Figure 1. Layout and dimensions of experimental vented deflagration test chamber [6]

Four pressure transducers were mounted to the inside of the chamber. The initial mixture was supplied by injecting the pure fuel through an inlet at floor level while mixing fans within the chamber were used to create a uniform mixture. Prior to ignition, the unburned mixture was contained within the chamber using a 0.02 mm thin sheet of polypropylene. Ignition was supplied using a carbon rod igniter. Pressure-time histories were provided, recorded by transducer P1. This allowed detailed comparison with simulation results permitting model analysis. The pressure recorded at this location

during the experiments and simulations will be labelled as 'Internal' in subsequent pressure-time graphs. Unfortunately, external pressure transients are not available.

3.0 THE MODEL OVERVIEW

The governing equations used during the simulations describing the combustion of the premixed, initially quiescent, hydrogen-air mixture are obtained by filtering the dimensional conservation equations of mass, momentum, energy and species concentration and are published elsewhere e.g. [7].

3.1 Premixed flame propagation modelling

The transport equation for the progress variable, which is defined as the mass fraction of the products of combustion, is applied for flame propagation tracking:

$$\frac{\partial}{\partial t}\left(\overline{\rho}\widetilde{c}\right)+\frac{\partial}{\partial x_j}\left(\overline{\rho}\widetilde{u}_j\widetilde{c}\right)=\frac{\partial}{\partial x_j}\left(\frac{\mu_{eff}}{Sc_{eff}}\frac{\partial\widetilde{c}}{\partial x_j}\right)+\overline{S}_c\,. \tag{1}$$

The source term in the progress variable equation can be written using the gradient method [8] as:

$$\overline{S}_c=\rho_u S_T\left|grad\ \widetilde{c}\right|, \tag{2}$$

where $|grad\,\tilde{c}|$ is the gradient of the progress variable. Using this method the integral of the source term through the numerical flame front thickness gives the same mass burning rate per unit flame surface area, $\rho_u S_T$, independent of the size of cells in the numerical front. Therefore, the calculation of the turbulent burning velocity is decoupled from the numerical mesh, for freely propagating flames. The numerical flame thickness typically spreads through three to five cells. An expression for the turbulent burning velocity, which is required to complete the gradient method calculation process, is described in the following section. The effective viscosity is calculated according to the renormalization group (RNG) theory [9]. The RNG model of turbulence does not contain any adjustable coefficients or ad hoc parameters. During the present simulations the molecular Prandtl number and Schmidt numbers are both set to 0.7, reflecting the characteristics for air. The effective Prandtl and Schmidt number is calculated according to RNG theory [9].

Due to the large scale, real world, experimental problems investigated in this study and the small scale of computational cells that would be required to resolve the associated reacting flow phenomena, the effects of turbulence and combustion instabilities, including RT instability, must be modelled in order to reproduce the experimental deflagration dynamics. This combustion model accounting for key phenomena, must be introduced to the simulations. In the present study such a model has been implemented through the utilisation of an appropriate UDF. This capability is available within the solver employed, ANSYS Fluent (release 13.0).

3.2 Multi-phenomena turbulent burning velocity model

The multi-phenomena turbulent burning velocity deflagration model exploited in this study is under continuous development. The latest version of this model is described in [1]. This version of the model takes into account various phenomena which are known to have a significant influence on the turbulent burning velocity. These phenomena include changes of pressure and temperature in the unburned gas, flow turbulence, turbulence generated by the flame front itself, Ξ_K, preferential diffusion of turbulent flames at different curvature radii (so-called leading point concept), Ξ_{lp}, and as large scale deflagration scenarios are under consideration, fractals increase of the turbulent flame surface area, Ξ_f. Following the inclusion of these different mechanisms the equation describing turbulent burning velocity is written as:

$$S_T = S_u^w \cdot exp(u'/S_T)^2 = \left[S_u \cdot \Xi_K \cdot \Xi_{lp} \cdot \Xi_f\right] \cdot exp(u'/S_T)^2 , \quad (3)$$

where u' is the SGS turbulent flow velocity [10], and S_T is the turbulent burning velocity. Equation 3 is a modified form of Yakhot's original equation [11] for turbulent premixed flame propagation velocity. The key step in the development of this model is the substitution of the laminar burning velocity term, S_u , in Yakhot's original equation with the sub-grid scale (SGS) wrinkled burning velocity, S_u^w. This introduced term, S_u^w, accounts for the unresolved phenomena within the simulations affecting burning rate at all SGS lengths. It should be noted that S_u^w influences the total turbulent burning rate through interaction with flow turbulence in the unburned mixture, which is accounted for within the modified form of Yakhot's equation, Eq. 3.

Each of the mechanisms included in this version of the model are described in detail in various publications, most notably [1]. Within the mechanisms contained within Eq. 3 are a number of parameters that must be defined. The dependence of the laminar burning velocity on transient pressure, p , and temperature, T, is taken into account within the model following the assumption of adiabatic compression / expansion. This requires the calculation of the thermokinetic index, ε, which is taken from [12], as $\varepsilon = 0.65$. Following [13] the characteristic radius at which transition to the fully turbulent self-similar regime, R_0, occurs is set to 1 m and finally the 'ad-hoc' parameter ψ contained with the model ($\psi < 1$) is set to 0.5 in the present study following [14].

3.3 Mesh geometry, initial and boundary conditions and numerical details

The calculation domain as partially shown below in Fig. 2 comprises a large hemispherical area of radius 25 m.

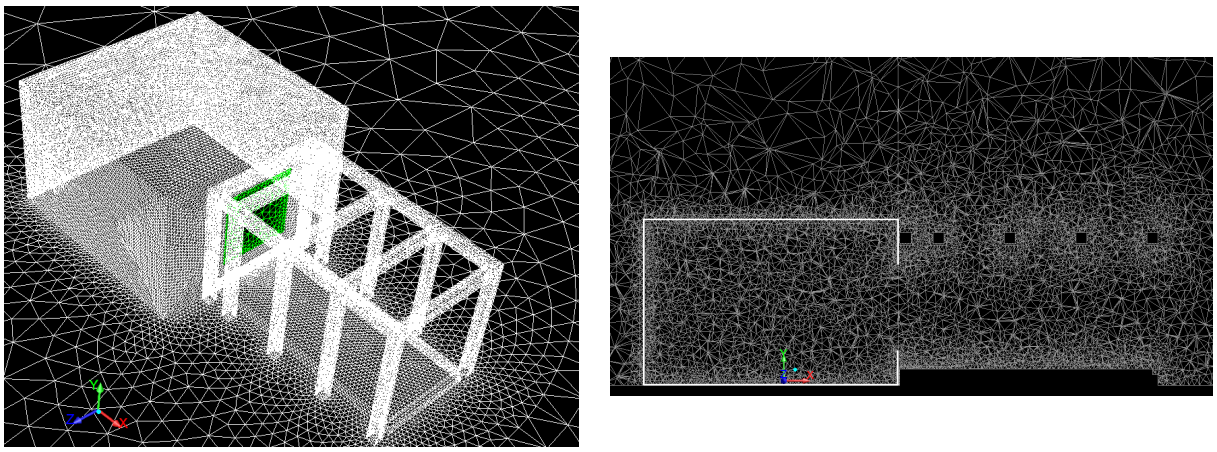

Figure 2. Computational domain, 3D representation (left); and cross-section of area of interest (right)

At the centre is a representation of the FM Global large scale deflagration facility [6]. This large area surrounding the chamber was created in order to exclude the effects of boundary conditions on the external deflagration and also to accommodate the diverging pressure wave generated. The calculation domain was meshed using an unstructured tetrahedral grid. Using this meshing option allows complex calculation domains to be meshed as it also allows the use of hexahedral, pyramidal and wedge elements where appropriate. During this analysis the smallest control volumes (CVs) were located inside the chamber and in the area immediately outside the vent, where the external deflagration takes place. The average edge size of the CVs located inside the chamber and around the vent was 0.1 m. This clearly implies the requirement for SGS modelling of unresolved combustion mechanisms as mentioned above. The characteristic CV size was then smoothly increased within the rest of the calculation domain. In the case of the 2.7 m^2 vent simulations the total number of CVs was 991,824 while in the 5.4 m^2 vent simulations the total number of CVs was 989,339. This was a similar total as

reported in [6]. The boundary conditions applied were non-slip, non-permeable, adiabatic conditions on all walls and ground surfaces. At the outer edge of the calculation domain the non-reflecting pressure far-field boundary condition, as implemented by ANSYS Fluent based on Riemann invariants, was applied. An unrestricted open vent was used in all simulations.

At initial conditions the flammable mixture was contained inside the chamber and air was located in the remaining area of the calculation domain. The pressure was set to atmospheric and initial temperature was 295 K. Inside the calculation domain the initial value of the progress variable was set to $c=0$. Inside the chamber the initial mass fraction of hydrogen was $Y_{H_2}=0.015$ (corresponding to 18% of hydrogen by volume) and the mass fraction of air was $Y_a=0.985$. Combustion was initiated by slowly increasing the progress variable in one CV (nearest to the experimental ignition location). The duration of ignition was assumed to be equal to the flame propagation time from the centre to the edge of the ignition CV: $\Delta t_{ign} = 1/2 \cdot (\Delta_{cv}/S_u \cdot E)$, where Δ_{cv} is the ignition CV size (equivalent radius).

As a tetrahedral mesh was implemented, in order to obtain more accurate results, the governing equations were solved by employing a second-order accurate upwind scheme for convection terms. Following authors' experience the reduction of discretization scheme from 2nd order to 1st order resulted in a significant decrease of combustion rate and an underestimation of pressure peaks. The diffusion terms were central-differenced and second-order accurate. The progress variable and energy source terms were solved within the UDF capability available when using ANSYS Fluent. An explicit scheme was used for time stepping, where the Courant-Friedrichs-Lewy (CFL) number was set to 0.8 to ensure stability. This resulted in a time step of the order of 10^{-6} s.

3.4 Simulation results prior to the inclusion of the Rayleigh-Taylor instability

The simulation results shown in Fig. 3 were obtained using the multi-phenomena turbulent burning velocity model described by Eq. 3. These results will subsequently be termed as the 'former' model results. Also plotted on Fig. 3 are the experimental internal pressure dynamics published in [6].

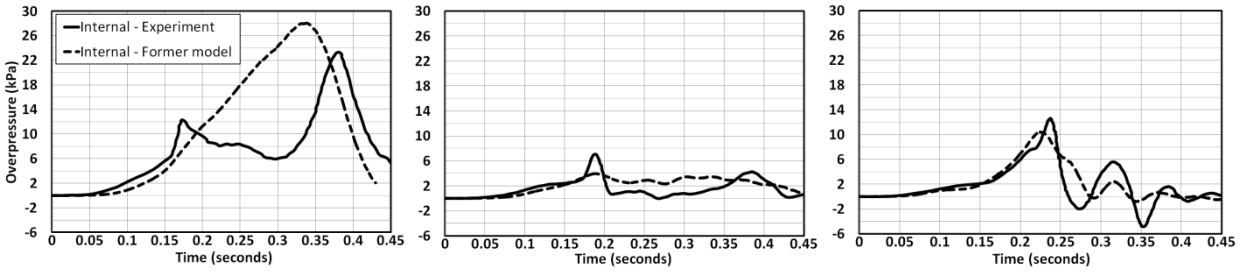

Figure 3. Comparison between experiment and former model simulations, central ignition case using the 2.7 m^2 vent (left); central ignition case using the 5.4 m^2 vent (centre); and back wall ignition case with the 5.4 m^2 vent (right)

As shown in Fig. 3, when considering the central ignition cases, the former model failed to satisfactorily reproduce the experimental pressure dynamics recorded during the vented deflagrations reported in [6]. However the model did perform well, showing general agreement with the maximum pressures and general shape of the experimental results, when considering the back wall ignition case. It is clear from these simulation results, particularly for the central ignition cases, that the first distinct pressure peak due to the external deflagration has not been reproduced.

From the literature [15] the first pressure peak can be said to be caused by the external deflagration, created by the flame front emerging from the vent and propagating through the unburned highly turbulent hydrogen-air mixture which had been previously expelled from the chamber. In order for the external deflagration to have a significant influence on the internal pressure dynamics, the pressure generated by this external explosion must be comparable to or above the internal pressure. Such a pressure increase externally will reduce the pressure difference across the vent and thereby cause a

reduction in the efficiency of venting throughout the duration of the external deflagration [1], [16]. This blocking of the outflow will cause the internal pressure to increase until the external deflagration pressure has dissipated. Following this dissipation the pressure inside will be released and the pressure peak will be generated. The importance of the "external explosion" during coherent vented deflagrations has been highlighted by Harrison and Eyre [17] who concluded that the extent to which the external explosion influences the internal chamber pressure depends on the relative magnitudes of the internal and external pressures. In some cases it was reported that the external deflagration can be the dominant influence on the internal pressure [17]. This is consistent with the findings described in [3]. The authors of [6] stated, following private communication, that during the experiments the external overpressures measured at a distance of 1.17 m from the centre of the vent were of comparable strength to the internal pressure measured at location P1 (Fig. 1). As shown in Fig. 4 the external pressures obtained from the former model at this external location were not of sufficient strength to have a significant influence on the internal pressure dynamics.

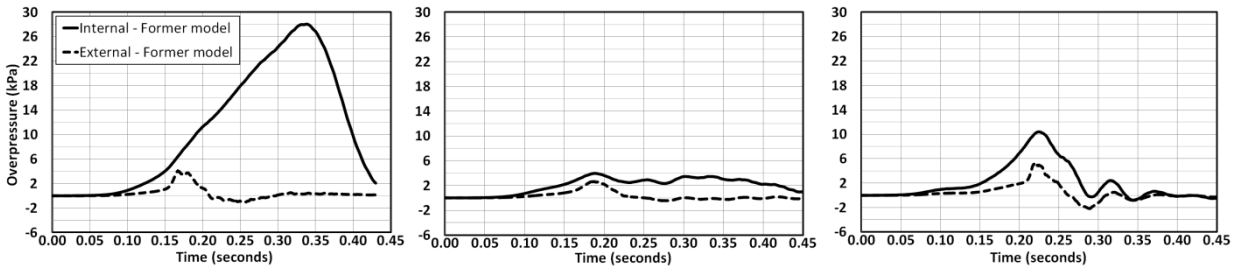

Figure 4. Former model internal and external pressure dynamics, central ignition case using the 2.7 m^2 vent (left); central ignition case using the 5.4 m^2 vent (centre); and back wall ignition case with the 5.4 m^2 vent (right)

This under-prediction can be attributed to the absence of a combustion enhancing mechanism causing the intensification of the external deflagration that not being accounted for within the former model.

4.0 MODELLING OF RAYLEIGH-TAYLOR INSTABILITY

The influence of Rayleigh-Taylor (RT) instability during vented deflagrations has been investigated by a number of authors. The growth of this instability has been found to occur most prominently as the flame accelerates through the vent [18] and also close to the vent following the expulsion of the hot combustion gases from the chamber [19]. Additionally, following previous work undertaken by authors [4], the flow conditions required for the growth of RT instability were identified following the application of the former model to analyse the experiments described in [5]. During this analysis the timings of the first and second experimental pressure peak were found to correspond with the flame accelerating as it flowed under the car and as it flowed from under the car. These conditions also fulfilled the requirements for the growth in RT instability. This result has provided the basis for the inclusion of RT instability during the simulation of vented deflagration scenarios. The derived mathematical model describing RT instability is detailed below.

4.1 Time-dependent RT instability model

Rayleigh-Taylor instability was first described mathematically by Lord Rayleigh [20] and then by Sir G. Taylor [21]. The first experiments to validate the theory were conducted by Lewis [22]. It occurs at the interface between two fluids of different densities when subjected to acceleration in the direction from the lighter to the heavier. Accelerations in the flow, as described by Zeldovich et al. [23], may vary periodically both in magnitude and sign and as such can have a periodic stabilizing and destabilizing effect on the flame front. Additionally, following the experimental observations described in [18] it has been assumed that the flame front takes on a needle-like structure when the RT instability becomes dominant. Taking these physical considerations into account the shape of the perturbed flame front has been simplified into cone shapes of differing heights. The RT instability

wrinkling factor itself will take the form of the ratio between the surface areas of the slanted side of this conic shape and the flat circular base, a representation of these two surface areas, S_1 and S_2, is shown in Fig. 5.

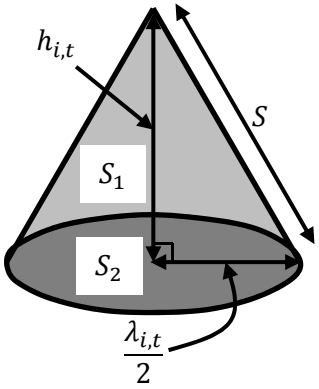

$$\Xi_{RT} = \frac{S_1}{S_2} = \frac{\pi \cdot (\lambda_{i,t}/2) \cdot S}{\pi \cdot (\lambda_{i,t}/2)^2} = \frac{S}{(\lambda_{i,t}/2)},$$

where $S = \sqrt{\left(\frac{\lambda_{i,t}}{2}\right)^2 + h_{i,t}^2}$.

Therefore: $\Xi_{RT} = \sqrt{1 + \left(\frac{h_{i,t}}{\lambda_{i,t}/2}\right)^2}$

Figure 5. Sketch of the shape of the RT perturbed element of the flame front.

The growth of the amplitude of the perturbation is described according to $h_{i,t}=h_{i,t-\Delta t} \cdot e^{\omega t}$ [23]. The growth rate is controlled by acceleration. However, the amplitude of the perturbation will increase only if acceleration is in the unstable direction (from lighter to heavier fluid). Conversely, annihilation of the flame surface at cusps [16], termed the 'sink', as well as a reduction in the amplitude if acceleration occurs in the opposite direction (from heavy to light) controls the reduction of the RT wrinkling factor down to one. Using Fig. 5, and following these considerations of the behaviour of the RT perturbation, the equation describing the growth and removal of the RT amplitude, $h_{i,t}$, can be written as:

$$h_{i,t} = h_{i,t-\Delta t}\left(1 + \omega_{i,t} \cdot \Delta t\right) - \alpha \cdot S_{T,i,t}\left(\Xi_{RT} - 1\right)\Delta t\,, \tag{4}$$

where $h_{i,t-\Delta t}$ is the amplitude of the perturbation at the previous timestep, $\omega_{i,t}$ is the growth rate and α is an empirical coefficient of the order of 1.0 associated with the removal term. Wavelength and growth rate, as defined in Eq. 5 and Eq. 6 respectively, are both dependent on acceleration, therefore as stated in [24] for a particular value of acceleration there is a specific, corresponding, most unstable wavelength. The equation for wavelength, $\lambda_{i,t}$, obtained from [24], as a function of acceleration is calculated according to:

$$\lambda_{i,t} = 4 \cdot \pi \cdot \left(\frac{\nu_{T,i,t}^2}{g_{i,t} \cdot A_{i,t}}\right)^{1/3}, \tag{5}$$

where $\nu_{T,i,t}$ is the turbulent kinematic viscosity, $A_{i,t}$ is the Atwood number and $g_{i,t}$ is the acceleration. Growth rate is calculated using the classical equation outlined by many authors, including [25]. Following substitution of Eq. 5 into the growth rate equation obtained from [25], growth rate, $\omega_{i,t}$, is written as:

$$\omega_{i,t} = \sqrt{A_{i,t} \cdot \frac{2 \cdot \pi}{\lambda_{i,t}} \cdot g_{i,t}} = \sqrt{\frac{\left(A_{i,t} \cdot g_{i,t}\right)^{4/3}}{2 \cdot \nu_{T,i,t}^{2/3}}}\,. \tag{6}$$

To take into account the change in acceleration, and recalling that the RT mechanism is a ratio between the perturbed and unperturbed flame surface area, the amplitude at each timestep is re-scaled according to the calculated value of wavelength (which depends on acceleration, Eq. 5) at the current and previous timestep. This rescaling is carried out prior to the calculation of the updated amplitude

described by Eq. 4. Furthermore Eq. 4 contains an empirical coefficient, α, associated with the 'sink' term, this coefficient is of the order of 1.0 and following parametric analysis is set to 0.75 in this study. The final term that should be considered is the calculation of an appropriate value of the initial perturbation amplitude. Initial amplitude is calculated as a percentage of the wavelength as outlined in [26] and is calculated as:

$$h_{0,i,t} = k_h \times \lambda_{i,t}\,, \tag{7}$$

where k_h is a constant multiplier. The key area of interest within this present study is the influence that the introduction of RT instability, into the deflagration model, has on the intensity of the external deflagration as the flame emerges from the chamber. As such, in the remaining chamber volume k_h is set to 0.001 in order to limit the growth of the RT perturbation outside this area. Following the calculation of the initial amplitude using Eq. 7, within the flame front, amplitude is subsequently calculated according to Eq. 4. The values of k_h and α selected during the simulations undertaken are provided in Table. 1.

Table 1. Parameters specified within each simulation.

Simulation number	Experimental setup		Location			
			Inside chamber		Outside chamber and around vent	
	Vent size, m^2	Ignition	k_h	α	k_h	α
1	2.7	Centre	0.001	0.75	0.5	0.75
2	5.4	Centre				
3	5.4	Back wall				

The selection of k_h by the inverse problem method in the key area of interest can be viewed as providing an adequate baseline from which the growth of the RT instability can occur, it should not in itself, without growth in amplitude, generate a significant change in the overall behaviour of the resulting pressure dynamics. Following an analysis of this procedure significant growth in the value of Ξ_{RT} was found to be reliant on and only encountered in areas where there was a sufficiently high concentration of acceleration in the unstable direction. Using the simulation results obtained from Simulation 1 (Table 1) the flame front had propagated substantially into the area where the value of k_h had been increased before a significant increase in the value of Ξ_{RT} was encountered. This growth coincided with a substantial increase in acceleration in the unstable direction.

Finally to complete the description of the RT model implemented, the transport equation for RT wrinkling factor introduced to model has to be described. This additional user-defined scalar (UDS) transport equation solves for the RT factor, Ξ_{RT}. The equation to solve for Ξ_{RT} is written as:

$$\frac{\partial \Xi_{RT}}{\partial t} + \left(U_i + S_{T,i}\right)\frac{\partial \Xi_{RT}}{\partial x_i} = S_{\Xi_{RT}}\,. \tag{8}$$

The first term in Eq. 8 is the unsteady term accounting for the accumulation of the UDS. The second term is the convection term which accounts for the transport of the UDS due to the velocity field and finally the third term is the source term which accounts for any sources or sinks that can either create or destroy the UDS. It should be noted that Eq. 8 is similar to the transport equation derived in [27].

The unsteady term, accounting for the accumulation of the UDS in each CV, is defined as:

$$\frac{\partial \Xi_{RT}}{\partial t} = \frac{\Xi_{RT(new)} - \Xi_{RT(previous)}}{\Delta t}\,. \tag{9}$$

The convection term, accounting for the transport of the UDS due to the flow velocity field and turbulent burning velocity, is defined as:

$$\left(U_i + S_{T,i}\right)\frac{\partial \Xi_{RT}}{\partial x_i} = \left(U_x + S_{T,x}\right)\frac{\partial \Xi_{RT}}{\partial x} + \left(U_y + S_{T,y}\right)\frac{\partial \Xi_{RT}}{\partial y} + \left(U_z + S_{T,z}\right)\frac{\partial \Xi_{RT}}{\partial z}. \quad (10)$$

As the source term in the transport equation to solve for Ξ_{RT} (Eq. 8) should describe the generation and suppression of the RT wrinkling factor at the flame front, within a given CV over time, the equation describing the source term is written in our model as:

$$S_{\Xi_{RT}} = \frac{d\,\Xi_{RT}}{d\,h_{i,t}} \cdot \frac{d\,h_{i,t}}{dt}, \quad (11)$$

where $\frac{d\,\Xi_{RT}}{d\,h_{i,t}} = \frac{2 \cdot h_{i,t}}{\lambda_{i,t}\sqrt{\left(\lambda_{i,t}/2\right)^2 + h_{i,t}^2}}$ and $\frac{d\,h_{i,t}}{dt} = h_{i,t} \cdot \omega_{i,t} - \alpha \cdot S_{T,i,t}\left(\Xi_{RT} - 1\right)$.

Finally, as the solver used is ANSYS Fluent, scalar source UDFs must compute the source term, $S_{\Xi_{RT}}$ along with its derivative $\partial S_{\Xi_{RT}} / \partial \Xi_{RT}$. This term is used within the solver to enhance the stability of the solution and help convergence rates. The solver automatically determines if the value obtained will aid stability. This term is defined as:

$$\frac{\partial S_{\Xi_{RT}}}{\partial \Xi_{RT}} = \frac{2 \cdot h_{i,t}\left(-\alpha \cdot S_{T,i,t}\right)}{\lambda_{i,t}\sqrt{\left(\lambda_{i,t}/2\right)^2 + h_{i,t}^2}}. \quad (12)$$

The results obtained from the implementation of this RT instability model into the former version of the multi-phenomena deflagration model are presented in the next section.

4.2 Simulation results following inclusion of the RT instability model

Figure 6 demonstrates that, following the introduction of the RT instability mechanism to the model, the simulation results have improved. In the 5.4 m^2 vent cases the magnitude of the internal pressure peak associated with the external deflagration has been more closely replicated.

Internal pressure dynamics

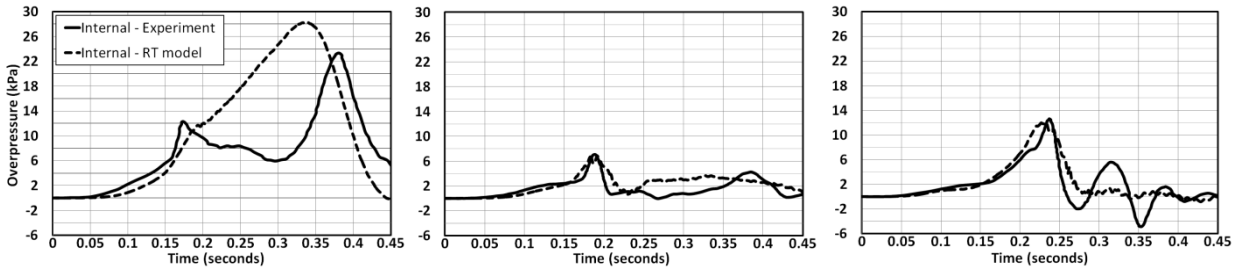

Figure 6. Comparison between experiment and RT model simulations, central ignition case using the 2.7 m^2 vent (left); central ignition case using the 5.4 m^2 vent (centre); and back wall ignition case with the 5.4 m^2 vent (right)

The general shape of the pressure-time curves produced from Simulation 2 (central ignition, 5.4 m^2 vent) and Simulation 3 (back wall ignition, 5.4 m^2 vent) agree quite closely with the experimental results. In Simulation 2 and Simulation 3, due to the implementation of the RT instability model, the sharp pressure increase associated with the external deflagration has been reproduced. Additionally in Simulation 2, following this peak, the decrease in pressure to near atmospheric levels has been replicated. In Simulation 1 (central ignition, 2.7 m^2 vent) the internal pressure peak associated with the external deflagration is more visibly reproduced. However following the external deflagration the simulation significantly over-predicts the internal chamber pressure prior to the second pressure peak.

It is worth noting that the second peak is mainly associated with the acoustic instability related to the chamber parameters, therefore its reproduction is beyond the scope of this preliminary study. The focus here is on the first peak related to coherent deflagrations inside and outside the chamber. The influence on the intensity of the external deflagration, due to the addition of the RT model, can be seen in Fig. 7.

External pressure dynamics

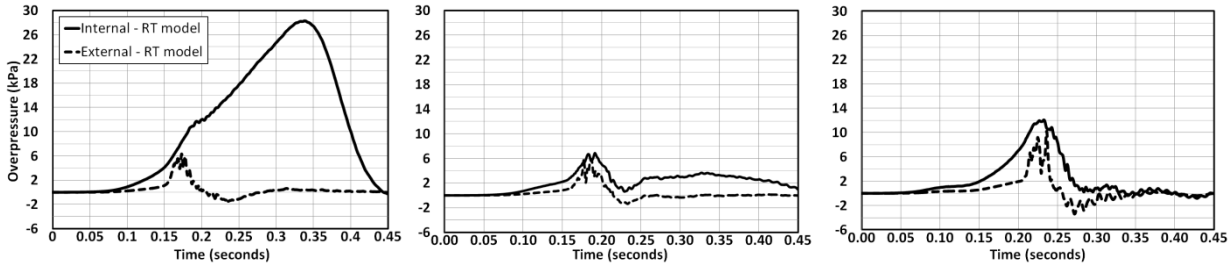

Figure 7. RT model internal and external pressure dynamics, central ignition case using the 2.7 m^2 vent (left); central ignition case using the 5.4 m^2 vent (centre); and back wall ignition case with the 5.4 m^2 vent (right)

As the flame exits the vent it accelerates the colder unburned hydrogen/air mixture, leading to the observed increase in Ξ_{RT}. This increase in Ξ_{RT} in the area surrounding the vent leads to an increase in flame surface area and ultimately the creation of the sharp external pressure peaks shown in Fig.7.

The results shown in Fig. 6 and Fig. 7 obtained from Simulation 1 (central ignition, 2.7 m^2 vent) indicate that the addition of the RT model has not had the desired influence on the magnitude of the external deflagration. As such an additional simulation has been undertaken to investigate the influence of increasing the value of k_h from 0.5 to 0.75. All other parameters have been kept constant. The results from this analysis are shown in Fig. 8.

Internal and External pressure dynamics

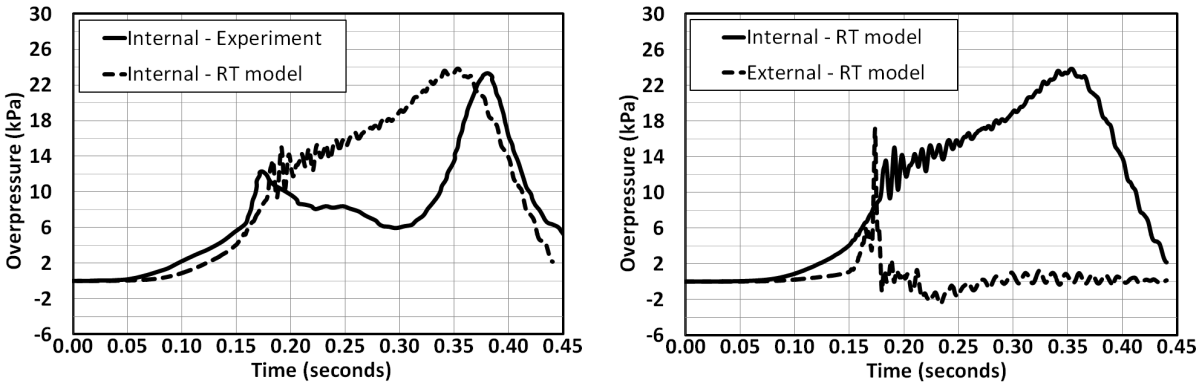

Figure 8. Central ignition case, 2.7 m^2 vent, $k_h = 0.75$ outside chamber and around vent: comparison between experiment and RT model (left); and internal and external pressure from RT model simulation (right)

The increase in k_h during this simulation has led to an increase in the magnitude of the external deflagration, which in turn has led to a more pronounced internal pressure peak. Overall this has led to closer agreement with the experimental results.

Prior to the addition of the RT instability model, as shown in Fig. 4, the external pressure was less than the internal pressure. However following the introduction of the RT model, and the subsequent

increase in the intensity of the external deflagration, the efficiency of the venting process was reduced. Consequently as the pressure outside the chamber was equal to or higher than the internal pressure, the pressure produced within the chamber was 'blocked' from escaping through the vent as efficiently as before. This resulted in the creation of the internal pressure peaks recorded during the simulations, following the addition of the RT model. After the external deflagration dissipated and the vent was 'unblocked' this increased pressure inside the chamber was then vented with a higher flow rate than before. Overall, this resulted in the simulated pressure-time curves coming into closer agreement with their corresponding experimental observations.

CONCLUSIONS

Rayleigh-Taylor instability was identified as playing a major role in pressure build-up during the external deflagration encountered within large scale scenarios. A model representing this instability has been developed and added to the multi-phenomena turbulent burning velocity deflagration model. The influence of this mechanism was limited to the external deflagration only in this study. This updated model was then tested against the experimental data obtained from large scale experiments on the vented deflagration of lean (18% by volume) hydrogen-air mixtures, undertaken by FM Global.

The model has been implemented in the form of a separate transport equation for the Ξ_{RT} wrinkling factor, containing source and sink terms developed based on phenomenological considerations of Rayleigh-Taylor instability. Following the addition of this mechanism the intensity of the external deflagration, as the flame reached and propagated through the vent, was substantially increased in each scenario investigated. As expected, this increase in pressure outside the chamber, in the area around the vent, had a significant influence on the internal pressure dynamics. The increased intensity of the external deflagration caused a decrease in the efficiency of the venting process, leading to an increase in the internal pressure. Following the fast dissipation of the external premixed combustion, the high pressure inside the chamber could be more efficiently vented. This process, now more closely captured following the introduction of the developed RT instability model, recreated the experimentally observed first pressure peak recorded during each experiment analysed within the scope of this study.

The introduction of RT instability into the multi-phenomena turbulent burning velocity deflagration model led to closer agreement between the simulated and experimental results. The addition of this mechanism was required in order to capture the main features and pressure transients associated with the coherent deflagrations that occurred in each investigated scenario. Therefore when considering the modelling of large scale vented deflagration scenarios, RT instability must be included as SGS premixed combustion sub-model.

REFERENCES

1. Molkov, V., Fundamentals of Hydrogen Safety Engineering, parts I & II. Free download e-book, www.bookboon.com, ISBN: 978-87-403-0279-0, 2012.
2. Keenan, J., Makarov, D. and Molkov, V., Towards the implementation of Rayleigh-Taylor instability into the multi-phenomena deflagration model, Proceedings of 7th ISFEH, Providence, R.I., USA, 2013, in print.
3. Molkov, V., Makarov, D. and Puttock, P., The nature and large eddy simulation of coherent deflagrations in a vented enclosure-atmosphere system, *Journal of Loss Prevention in the Process Industries*, **vol. 19**, no. 2–3, pp. 121–9, Mar. 2006.
4. Makarov, D., Verbecke, F., Molkov, V. and Keenan, J., On Unresolved Mechanisms of Large Scale Deflagrations in Complex Geometries, Proceedings of 6th ISFEH, U.K, 2010, pp. 93–103.
5. Shirvill, L. C., Royle, M. and Roberts, T. A., Hydrogen releases ignited in a simulated vehicle refuelling environment, presented at the 2nd ICHS, San Sebastian, Spain, 2007.
6. Bauwens, C. R., Chaffee, J. and Dorofeev, S.B., Vented explosion overpressures from combustion of hydrogen and hydrocarbon mixtures, *IJHE*, **vol. 36**, no. 3, pp. 2329–2336, Feb. 2011.

7. Molkov, V., Makarov, D. and Schneider, H., LES modelling of an unconfined large-scale hydrogen-air deflagration, *Journal of Physics D*, **vol. 39**, no. 20, pp. 4366–76, Oct. 2006.
8. Prudnikov, A., Combustion of homogeneous fuel-air mixtures in turbulent flows., Physical Principles of the Working Process in Combustion Chambers of Jet Engines, pp. 244-336, 1967.
9. Yakhot, V. and Orszag, S.A., Renormalization group analysis of turbulence. I. Basic theory, *Journal of Scientific Computing*, **vol. 1**, no. 1, pp. 3–51, 1986.
10. Pope, S. B., Turbulent Flows. Cambridge University Press, 2000.
11. Yakhot, V., Propagation velocity of premixed turbulent flames, *Combustion Science and Technology*, **vol. 60**, pp. 191–214, 1988.
12. Babkin, V. S., Private communication. Institute of Chemical Kinetics and Combustion, Siberian Branch, Russian Academy of Science, Novosibirsk, Russia, 2003.
13. Gostintsev, Y. A., Istratov, A. G. and Shulenin, Y. V., Self-similar propagation of a free turbulent flame in mixed gas mixtures, *Combustion, Explosion and Shock Waves*, **vol. 24** (5), 1989.
14. Verbecke, F., Formation and Combustion of Non-Uniform Hydrogen-Air Mixtures, PhD Thesis, HySAFER centre, University of Ulster, Newtownabbey, N. Ireland, U.K., 2009.
15. Cooper, M. G., Fairweather, M. and Tite, J. P., On the mechanisms of pressure generation in vented explosions, *Combustion and Flame*, **vol. 65**, no. 1, pp. 1–14, 1986.
16. Bauwens, C. R., and Dorofeev, S. B., Effect of the external explosion on vented deflagrations, presented at the 8th ISHPMIE, Yokohama, Japan, 2010.
17. Harrison, J. and Eyre, J. A., External Explosions' as a Result of Explosion Venting, *Combustion Science and Technology*, **vol. 52**, no. 1, pp. 91 – 106, 1987.
18. Tsuruda, T. and Hirano, T., Growth of Flame Front Turbulence during Flame Propagation across an Obstacle, *Combustion Science and Technology*, **vol. 51**, no. 4–6, pp. 323–328, 1987.
19. Solberg, D. M., Pappas, J. A. and Skramstad, E., Observations of flame instabilities in large scale vented gas explosions, *Symposium (Int.) on Combustion*, **vol. 18**, no. 1, pp. 1607–1614, 1981.
20. Lord Rayleigh, Proceedings of the London Mathematical Society 14 (1883), pp. 170-177; also, Scientific Papers, **vol. 2**, Cambridge U.P, pp. 200-207, 1883.
21. Taylor, G. I., The instability of liquid surfaces when accelerated in a direction perpendicular to their planes, I, Proceedings of the Royal Society of London, **vol. 201**, Series A, Mathematical and Physical Sciences, No. 1065, pp. 192 – 196, Mar. 1950.
22. Lewis, D. J., The instability of liquid surfaces when accelerated in a direction perpendicular to their planes, II, Proceedings of the Royal Society of London, **vol. 202**, Series A, Mathematical and Physical Sciences, No. 1068, pp. 81–96, Jun. 1950.
23. Zeldovich, Y. B., Barenblatt, G. I., Librovich, V. B. and Makhviladze, G. M., Mathematical theory of combustion and explosions, New York, NY, USA: Consultants Bur, 1985.
24. Youngs, D. L., Numerical simulation of turbulent mixing by Rayleigh-Taylor instability, *Physica D: Nonlinear Phenomena*, **vol. 12**, no. 1–3, pp. 32–44, Jul. 1984.
25. Dimonte, G., Ramaprabhu, P., Youngs, D. L., Andrews, M. J. and Rosner, R., Recent advances in the turbulent Rayleigh-Taylor instability, *Physics of Plasmas*, **vol. 12**, no. 056301, pp. 1–6, 2005.
26. Tryggvason, G., Numerical simulations of the Rayleigh-Taylor instability, *Journal of Computational Physics*, **vol. 75**, no. 2, pp. 253–82, Apr. 1988.
27. Weller, H. G., Tabor, G., Gosman, A. and Fureby, C., Application of a flame-wrinkling LES combustion model to a turbulent mixing layer, *Sym. (Int.) on Combustion*, **vol. 1**, pp. 899–907, 1998.